X-621-66-362

NASA TM X-55599

GLOBAL BEHAVIOR OF THE IONOSPHERE AT 1,000 KILOMETERS ALTITUDE

BY
L. H. BRACE
B. M. REDDY
H. G. MAYR

AUGUST 1966

NASA — GODDARD SPACE FLIGHT CENTER
GREENBELT, MARYLAND

GLOBAL BEHAVIOR OF THE IONOSPHERE AT 1,000 KILOMETERS ALTITUDE

BY

L. H. BRACE

B. M. REDDY*

H. G. MAYR*

Aeronomy Branch, Goddard Space Flight Center

Greenbelt, Maryland

*NASA-NRC resident research associate.

ABSTRACT

11374

Explorer XXII electrostatic probe measurements of electron temperature (T_e) and concentration (N_e) at the 1,000 kilometer level during the period from November 1964 to May 1965 are presented and discussed. Precession of the orbital plane during this period has permitted the resolution of two full diurnal cycles of ionospheric behavior at this altitude, one centered on the winter solstice and one on the vernal equinox. In both seasons, the latitudinal distributions of N_e and T_e reveal a diurnal modulation at middle and low latitudes which appears consistent with a mechanism of thermal expansion and contraction of the protonosphere along the geomagnetic field lines. Although there is a strong tendency toward symmetry about the magnetic equator, an important seasonal effect is evident as an enchancement of N_e throughout the summer hemisphere. Interpretation of the equatorial measurements in terms of the processes of photoelectron heating, local cooling via ions to neutrals, and electron thermal conduction permits the conclusions that:

1. diffusive equilibrium exists in the equatorial protonosphere, even at sunrise and sunset
2. the observed latitudinal distributions of T_e and N_e near the equator are mutually consistent with diffusive equilibrium, both day and night
3. a local electron cooling exists in the equatorial region which is inconsistent with present neutral atmosphere models but suggests the existence of about 5×10^5 cm^{-3} atoms of neutral hydrogen at 1,000 kilometers.

Author

CONTENTS

INTRODUCTION

In October 1964, the Explorer XXII satellite was launched into a 1,000 kilometer near circular orbit having an inclination of 80°. Brace and Reddy (1965) have reported initial measurements of electron concentraion (N_e) and temperature (T_e) by means of the electrostatic probe experiment on that satellite. Most of these early measurements were made during a three week period in November and December 1964, shortly after launch, when the orientation of the orbit relative to the sun permitted only midday and midnight sampling. From these data it was possible to examine the entire latitudinal distribution near 1,000 kilometers and at several longitudes. Comparison of the day and night distributions of T_e and N_e led to the conclusion that some kind of diurnal expansion and contraction was occurring. It was proposed that the observed behavior is consistent with a dynamic balance between heating by escaping photoelectrons and cooling by electron thermal conduction to the lower atmosphere.

Since the earlier paper, a great deal more data have been analyzed, and precession of the orbit has made it possible to resolve the detailed diurnal behavior of the ionosphere at this altitude during each of two consecutive seasons. The first of these diurnal cycles was centered on the 1964-65 winter solstice and the second corresponded to the 1965 spring equinox.

It is the purpose of this paper to report these new results and discuss their implications, particularly with regard to the processes which control the structure and behavior of the topside ionosphere. The data presented are limited to latitudes generally below 70° magnetic latitude, since polar cap results will be reported separately in a later paper.

EXPERIMENT DESCRIPTION

Cylindrical electrostatic probes of the type carried by Explorer XXII have been employed previously on a number of satellites and rockets and discussed in some detail elsewhere (Spencer, et al., 1962; Brace et al., 1963; Brace et al., 1965; Spencer, et al., 1965). The technique employs a long, thin cylindrical collector (23 cm × 0.06 cm) which is immersed in the plasma surrounding the satellite as it travels through the ionosphere. Figure 1 shows the physical and electrical configuration of the experiment. A 12 cm guard electrode is employed to permit the collector to protrude well into the plasma thus avoiding the disturbed region immediately adjacent to the satellite. As shown in the figure, a probe sensor is mounted on each end of the satellite. These are employed alternately to assure that non-wake measurements are available at all times.

The satellite is a large and relatively good conductor and therefore acts as a stable potential reference from which a 2 cps sawtooth voltage (-3 to +5v) is applied to the collector and guard. The resulting flow of ions and electrons to the collector produces a current waveform which is detected and telemetered to ground stations where the information is recorded on magnetic tapes. Microfilm analog displays of the volt-ampere characteristics are produced, and these data are reduced to T_e and N_e by use of conventional Langmuir probe theory discussed elsewhere (Spencer, et al., 1965).

The format of the raw data is illustrated in figure 2, which is a photograph of two consecutive sections of telemetry record representing a total of 10 seconds of data. The upper trace represents 5 seconds of data from the high current range (0.3 μa full scale), and the lower trace shows the following 5 seconds from the low current range (0.05 μa). An in-flight current calibration waveform

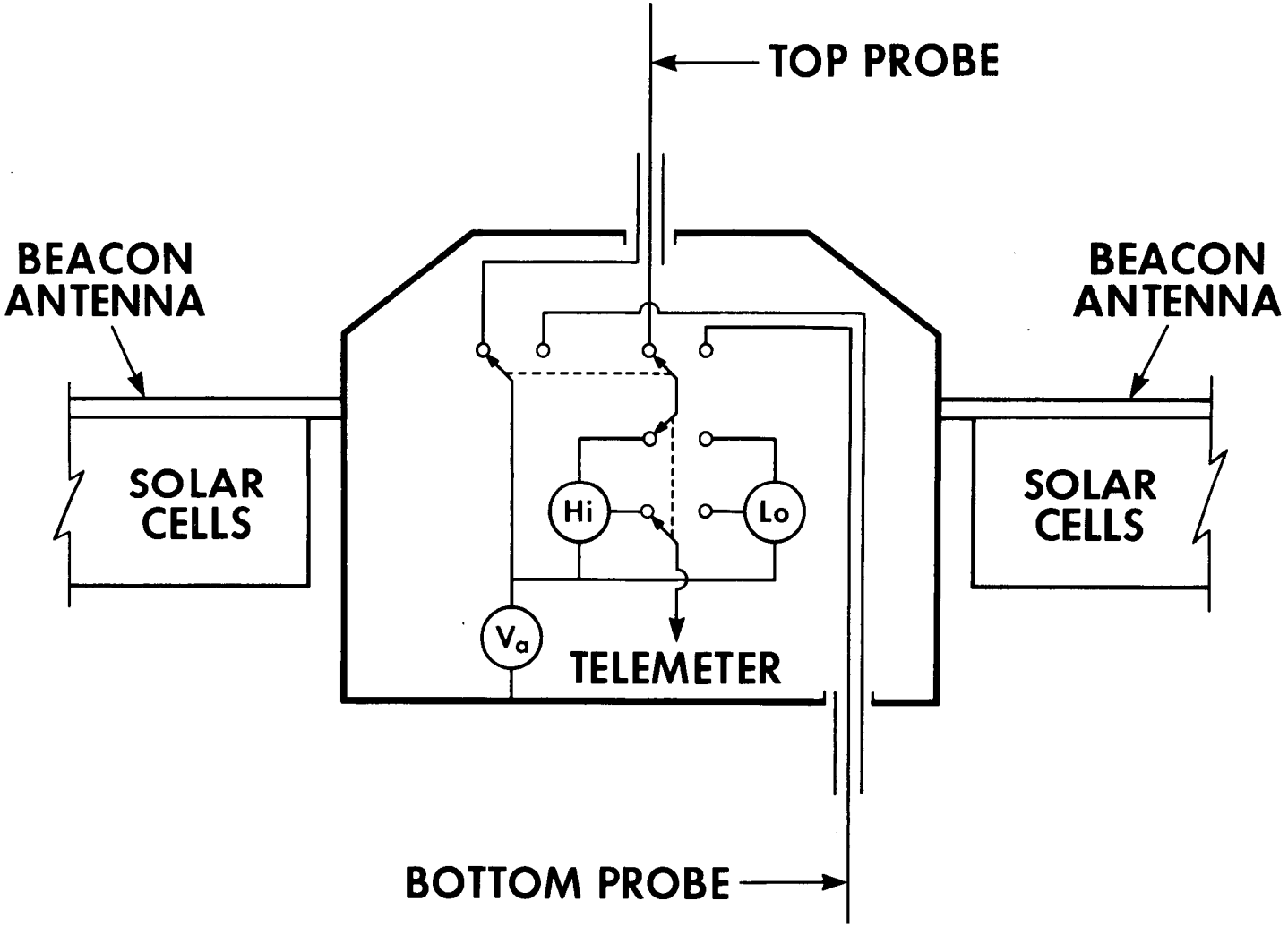

Figure 1 – Functional block diagram showing the electrical system and the mounting position of the probes. The sawtooth voltage, V_a, is applied alternately to the two probes, and the resulting volt-ampere characteristics are detected by either of two independent, linear current detectors.

EXPLORER XXII
RAW ELECTROSTATIC PROBE DATA

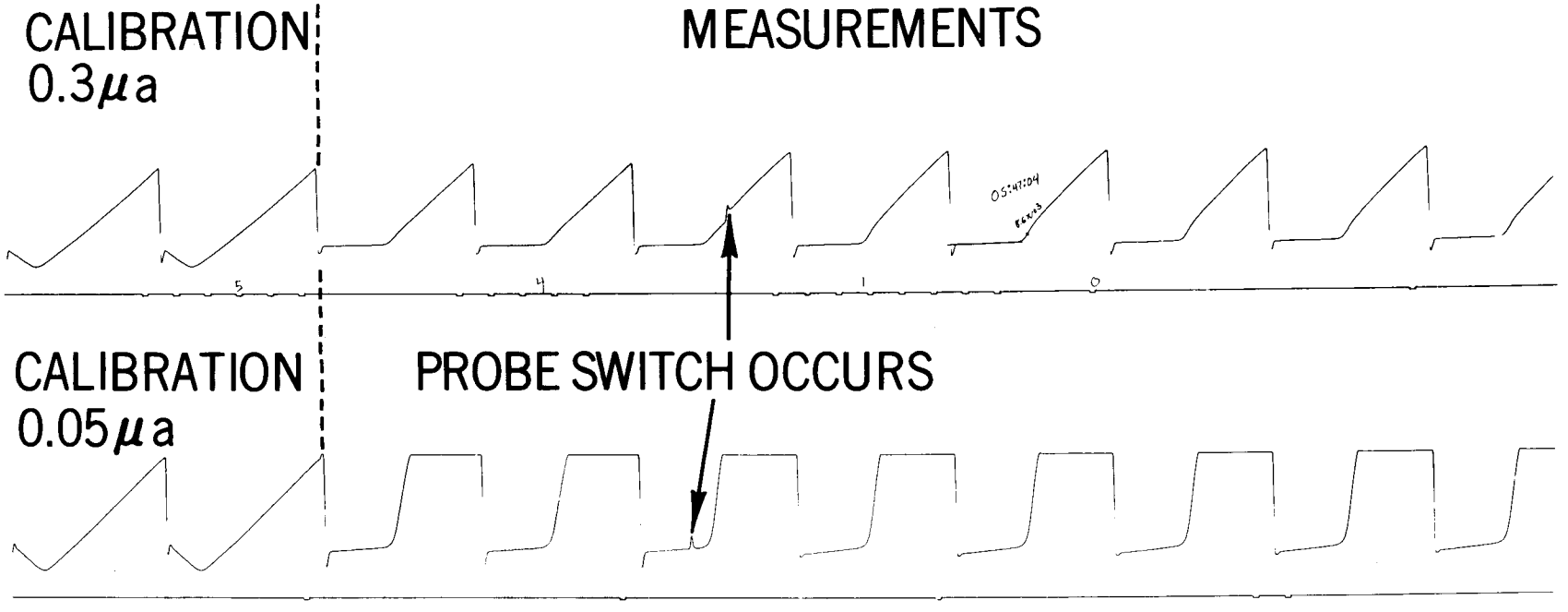

Figure 2 – Photograph of raw telemetry data showing 10 seconds of analog recording. Each current sensitivity is in-flight calibrated (waveforms at the left) and then connected in sequence to the two probes for measurement of their volt-ampere characteristic (waveforms on the right). The entire sequence requires 10 seconds and is repeated twice during each on-period.

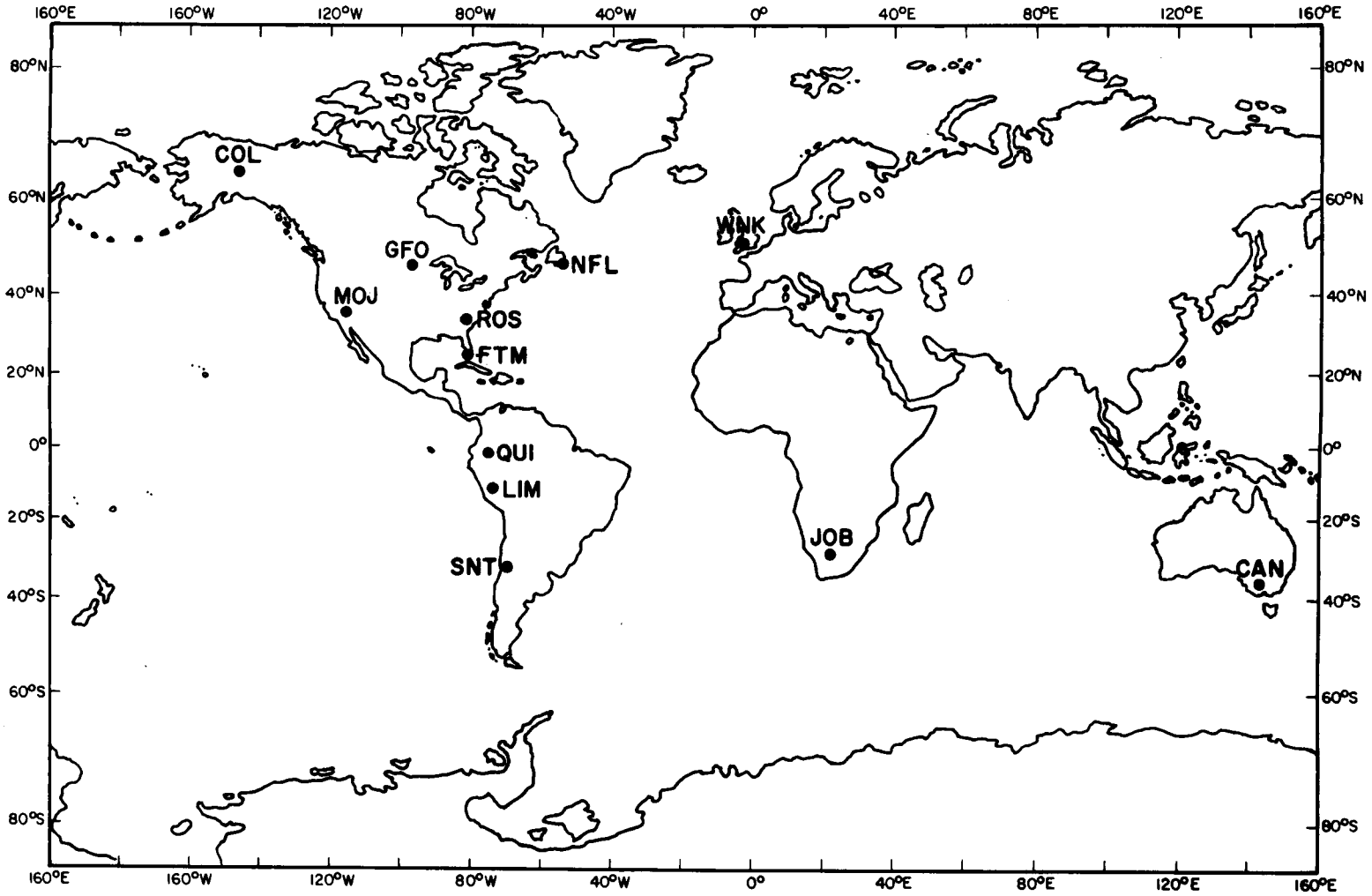

Figure 3 – Locations of the STADAN tracking and telemetry stations employed by the Explorer XXII satellite.

precedes each series of volt-ampere characteristics and the alternate probe is switched into the measurement circuit about midway in each 5 second series of curves. At normal electron concentrations, the entire volt-ampere characteristic is resolved on the high current channel, and the current in the electron saturation region is employed as a measure of the electron concentration. The low current channel permits a factor of six amplification of the same waveforms so that the electron retardation region of each characteristic can be resolved. The latter permits a determination of the electron temperature to be made.

It is important to note that, while the appropriate range of current sensitivity is being employed (alternate 5 second intervals), the electron temperature and concentration can be measured at half-second intervals. In terms of distance along the satellite path, this corresponds to about 4 kilometers. Thus large scale irregularities in electron concentration, which are sometimes seen, appear as a modulation envelope of the series of volt-ampere curves. Small scale irregularities, which are often seen in the polar region, appear as amplitude modulations within the individual curves themselves. Small scale irregularities having horizontal dimensions of about 50 meters have been observed in this manner.

The Explorer XXII satellite was designed to operate continuously so that no command capability would be required to permit global observation of the beacons and recording of the telemetry data. Since there is insufficient power to operate the probe electronics continually, it is turned on for 22 second periods at intervals of three minutes. This continues for 24 hours a day

throughout the life of the satellite (still operating at this writing). Owing to practical limitations, the telemetry data are recorded only about 4 hours per day as the satellite passes near STADAN tracking and telemetry stations. The stations employed for data recovery and their location are shown on the map in figure 3.

A result of the limited duty cycle employed is that the measurements of T_e and N_e are made along 150 kilometer segments of the orbit, and these segments occur at 1,200 kilometer intervals along the orbit. Although it is often possible to detect gradients of T_e and N_e within each segment or burst of data, our procedure has been to derive single values of T_e and N_e from each 22 second burst. Thus measurements are taken at 3 minute intervals which, in this near polar orbit, correspond to latitudinal increments of about 10°.

THE RESULTS

Figures 4 and 5 show the daytime values of N_e and T_e derived in the manner described above from about three weeks of data. During this period the orbit precessed by about 3 hours of local time. To aid in identifying the instantaneous latitudinal structure of the 1,000 kilometer level, the series of points corresponding to a single pass are joined by lines. Approximately 50 passes are shown here, which represent about half of the points available in this period. Measurements at different longitudes are coded differently as explained in the captions. However, longitudinal differences are comparatively less important than latitudinal and local time variations and will not be discussed further in this paper. In general, full latitude coverage was recorded only at the US longitudes (-50° to -100°) so that all results not otherwise identified will refer to this zone.

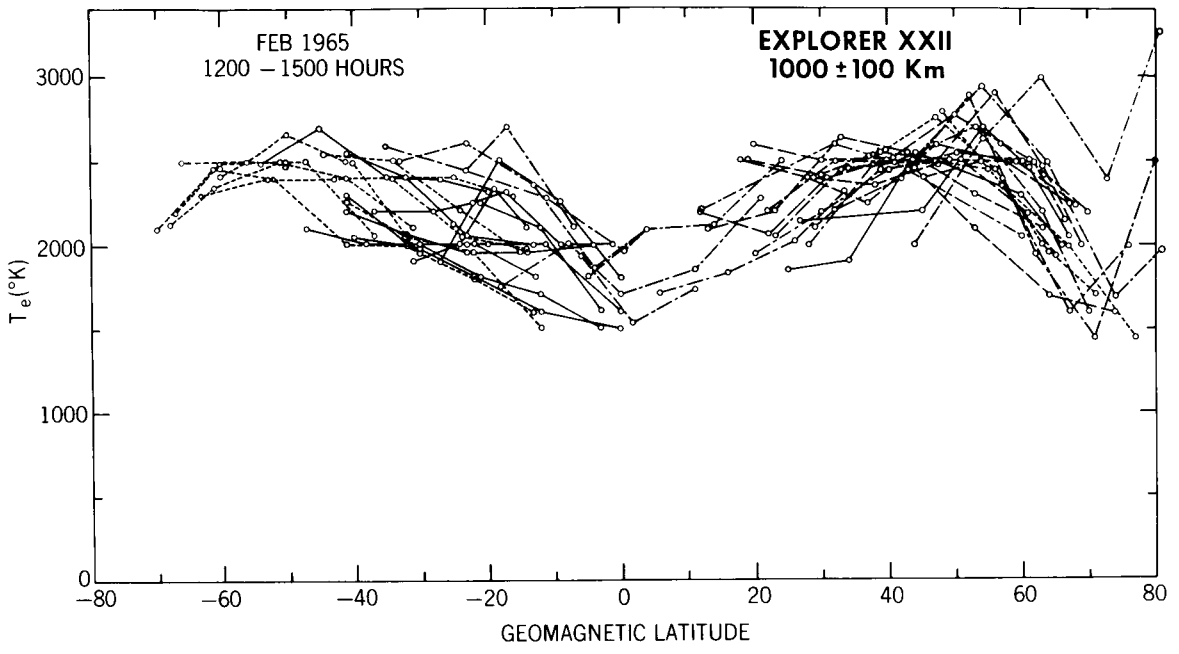

Figure 4 – Actual T_e data points derived from about 50 daytime satellite passes recorded in a three week period in February 1965. The points derived from a single pass are joined by lines to approximate the instantaneous latitudinal structure. The solid lines identify data from the longitude range (50°E - 50°W), the long dashes (100°W - 130°W), the short dashes (110°E - 150°E) and the long and short dashes (50°W - 100°W).

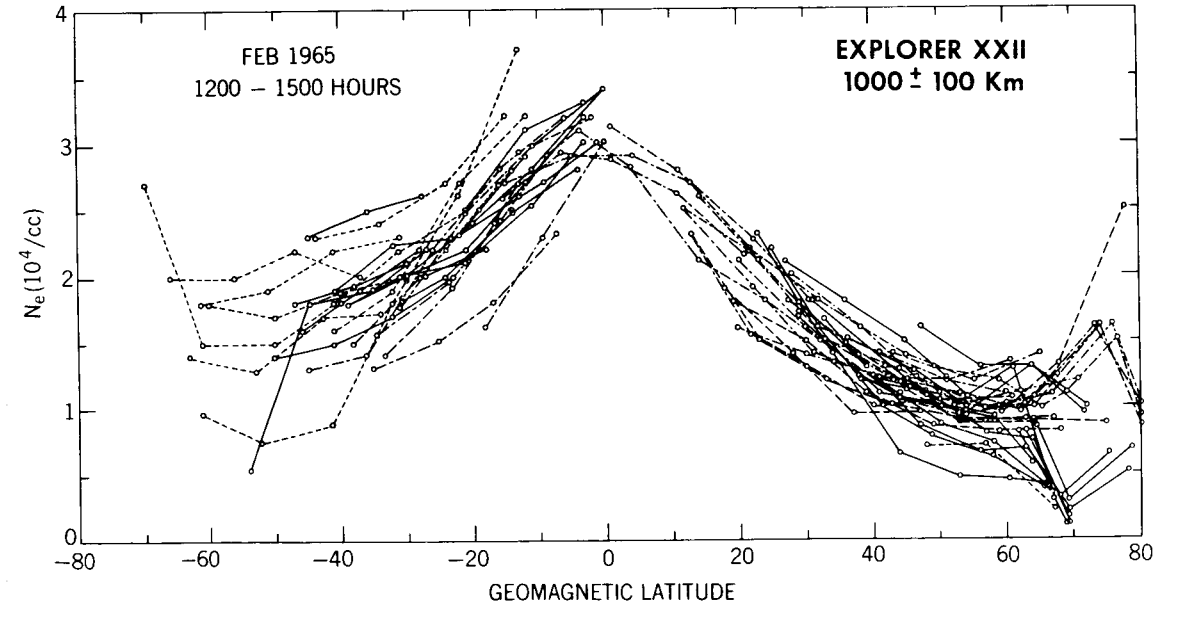

Figure 5 – Actual N_e data points derived from the same passes as discussed in figure 4.

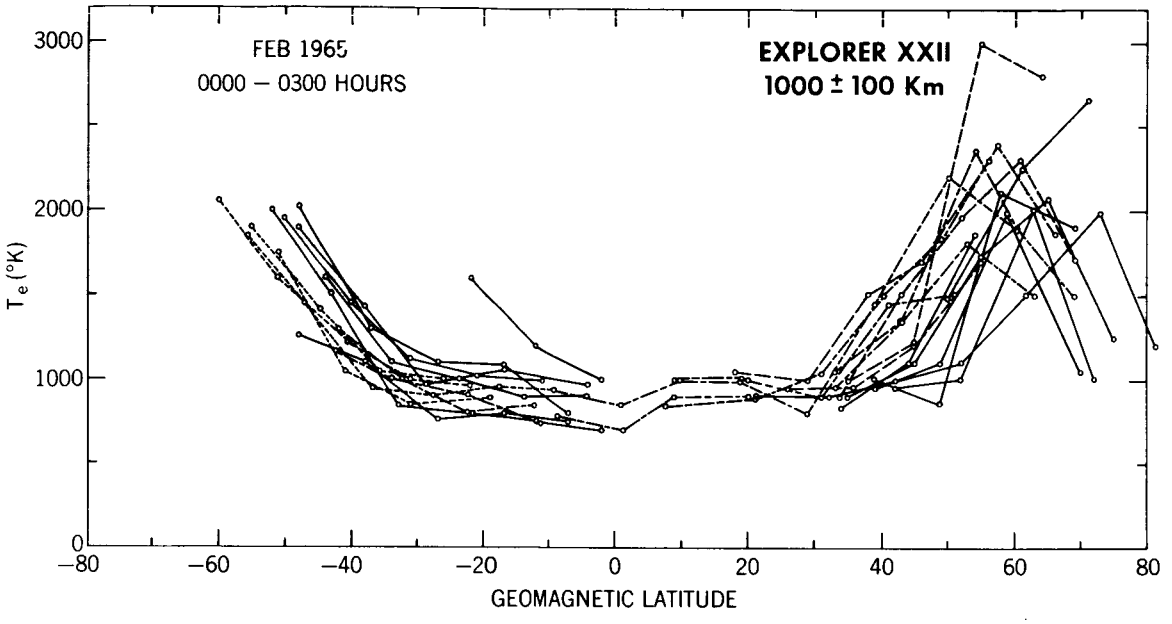

Figure 6 – Actual T_e data points from nighttime passes in the same three week period as of figures 4 and 5.

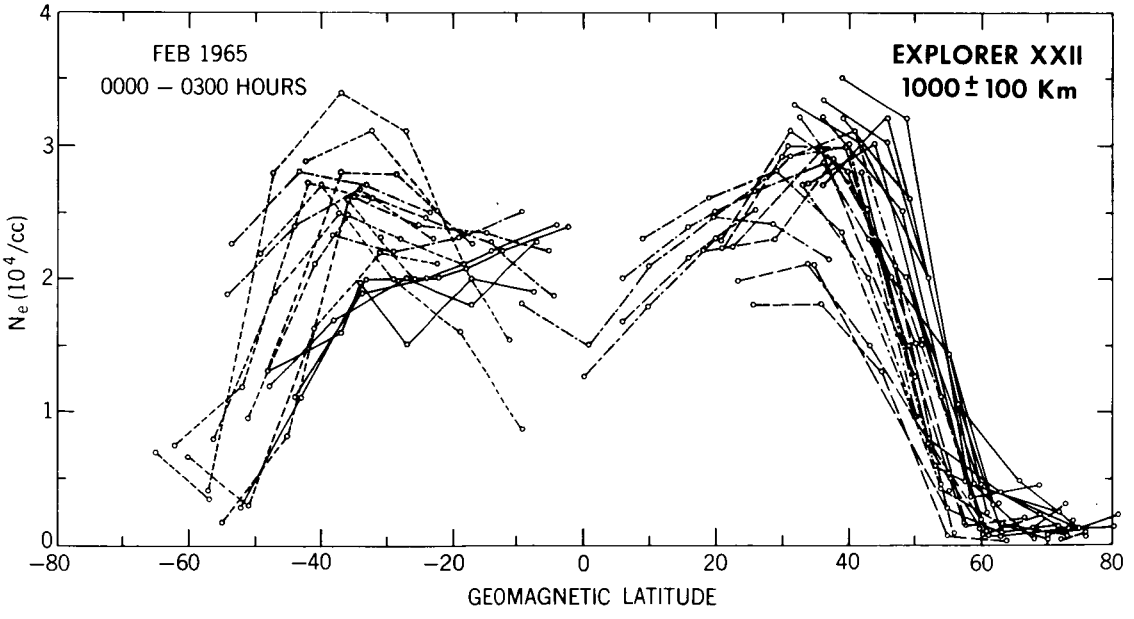

Figure 7 – Actual N_e data points corresponding to T_e data in figure 6.

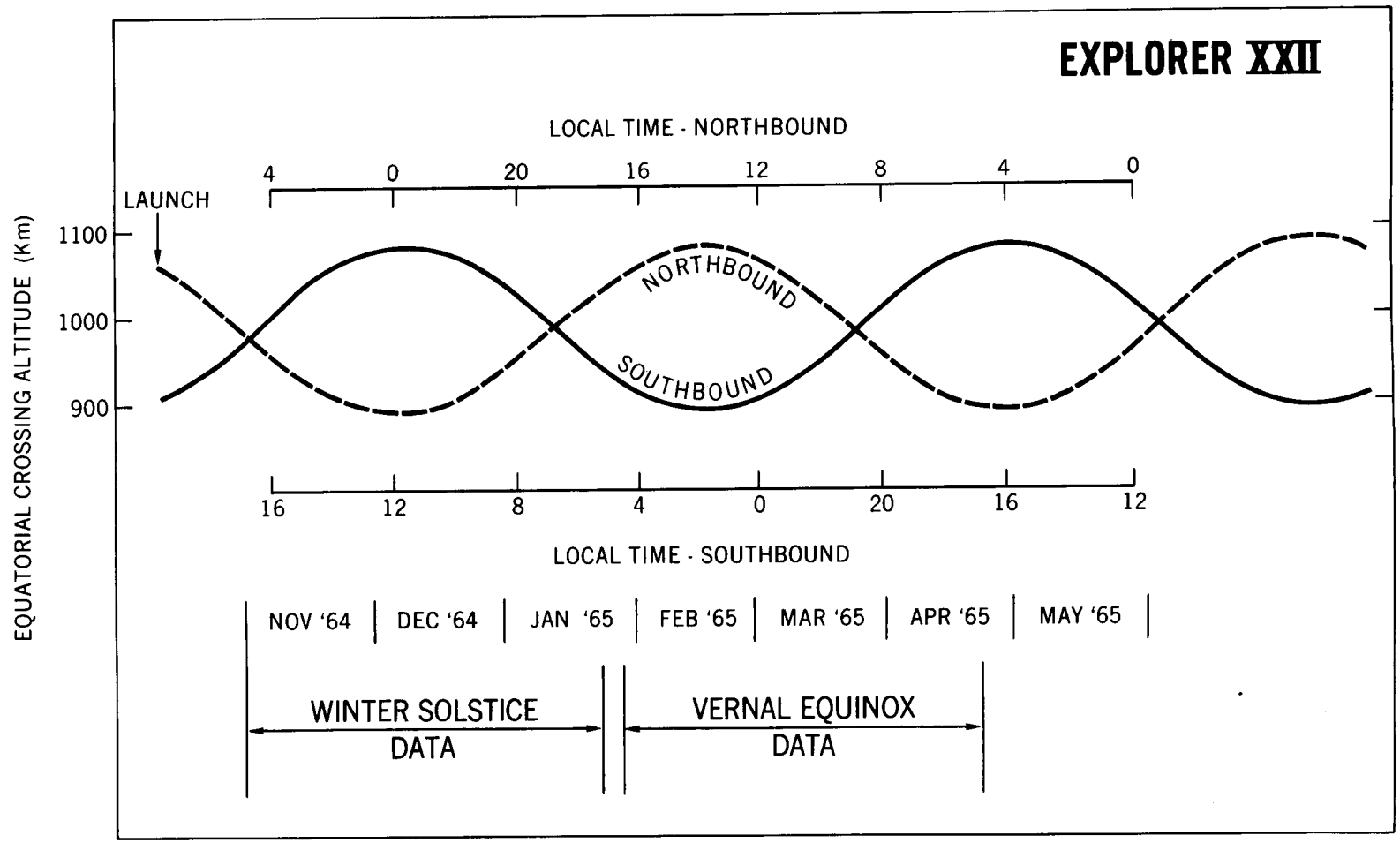

Figure 8 – Relationship between the satellite altitude and local time in the period for which data are reported here. The altitude scale has been expanded to permit its variation to be resolved. The northbound and southbound passes have been combined to permit a full diurnal cycle to be resolved in each of the indicated periods centered on the winter solstice and vernal equinox.

Figure 6 and 7 show the nighttime measurements for the corresponding three week period.

Point plots similar to those shown in figures 4 through 7 have been made for consecutive two-hour intervals throughout the two full diurnal cycles occurring between November 1964 and May 1965. Since the generation of each diurnal cycle is completed within a 3-month period, these data represent two seasons, winter and spring. The relationship between the altitude, season and local time for the equator is shown in figure 8. Note that the altitude scale is expanded.

A comment about the deviation of the Explorer XXII orbit from circularity is in order. When apogee (1,100 km) and perigee (900 km) are near the equator the difference between daytime and nighttime altitudes is greatest. However, during the period of the measurements reported here, the average nightside altitude was only about 100 kilometers lower than the average dayside altitude. This altitude difference should not be significant at the low and middle latitudes discussed here since, at 1,000 kilometers, the nighttime scale heights exceed 1,000 kilometers (Watt 1965, Thomas, et al., 1966). Therefore, in organizing the data for interpretation, it has been assumed that the altitudinal variations of N_e and T_e can be neglected.

The data in each two-hour local time period have been averaged and plotted as a family of latitudinal profiles. Figures 9 and 10 show the resulting average behavior for the winter period of 1964-65, and figures 11 and 12 show the summary of the spring 1965 data. These figures represent an attempt to summarize in a three dimensional fashion the dynamic behavior of the ionosphere at the 1,000 kilometer level during the periods of solstice and equinox.

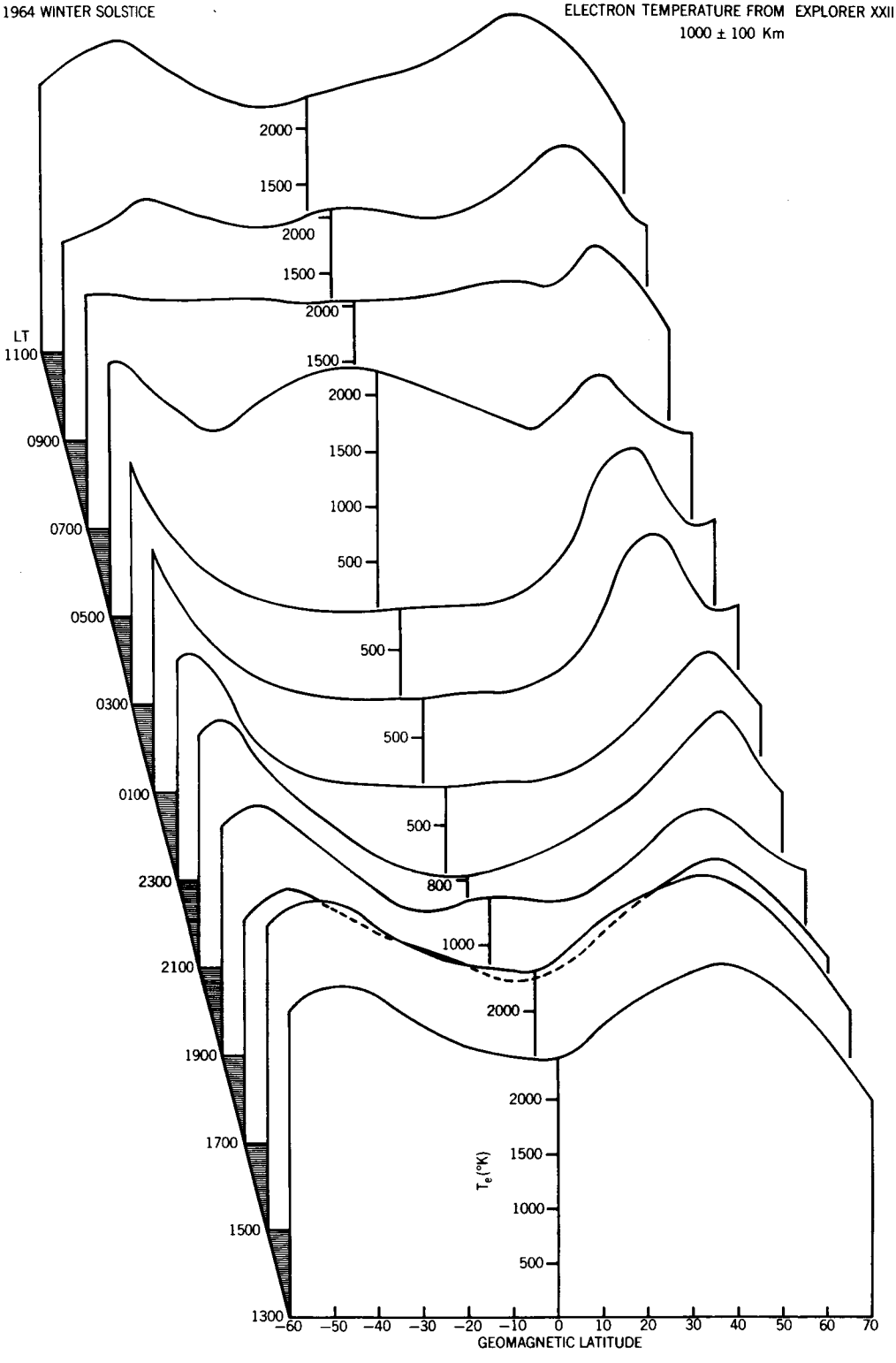

Figure 9 – Three dimensional model of the averaged latitudinal and local time behavior of T_e at the 1,000 kilometer level, in the winter solstice period.

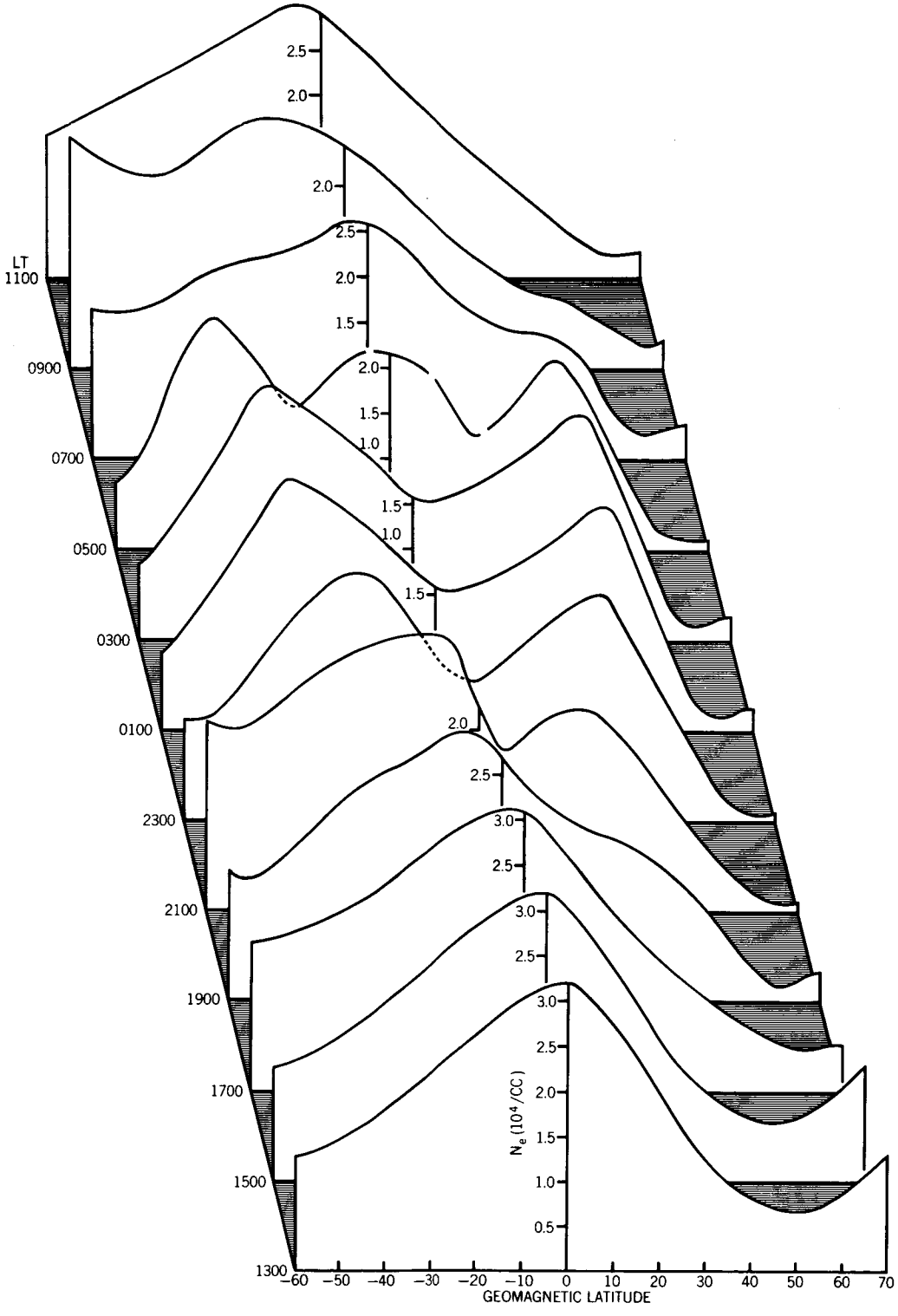

Figure 10 – Averaged variation of N_e at the 1,000 kilometer level corresponding to T_e data of figure 9.

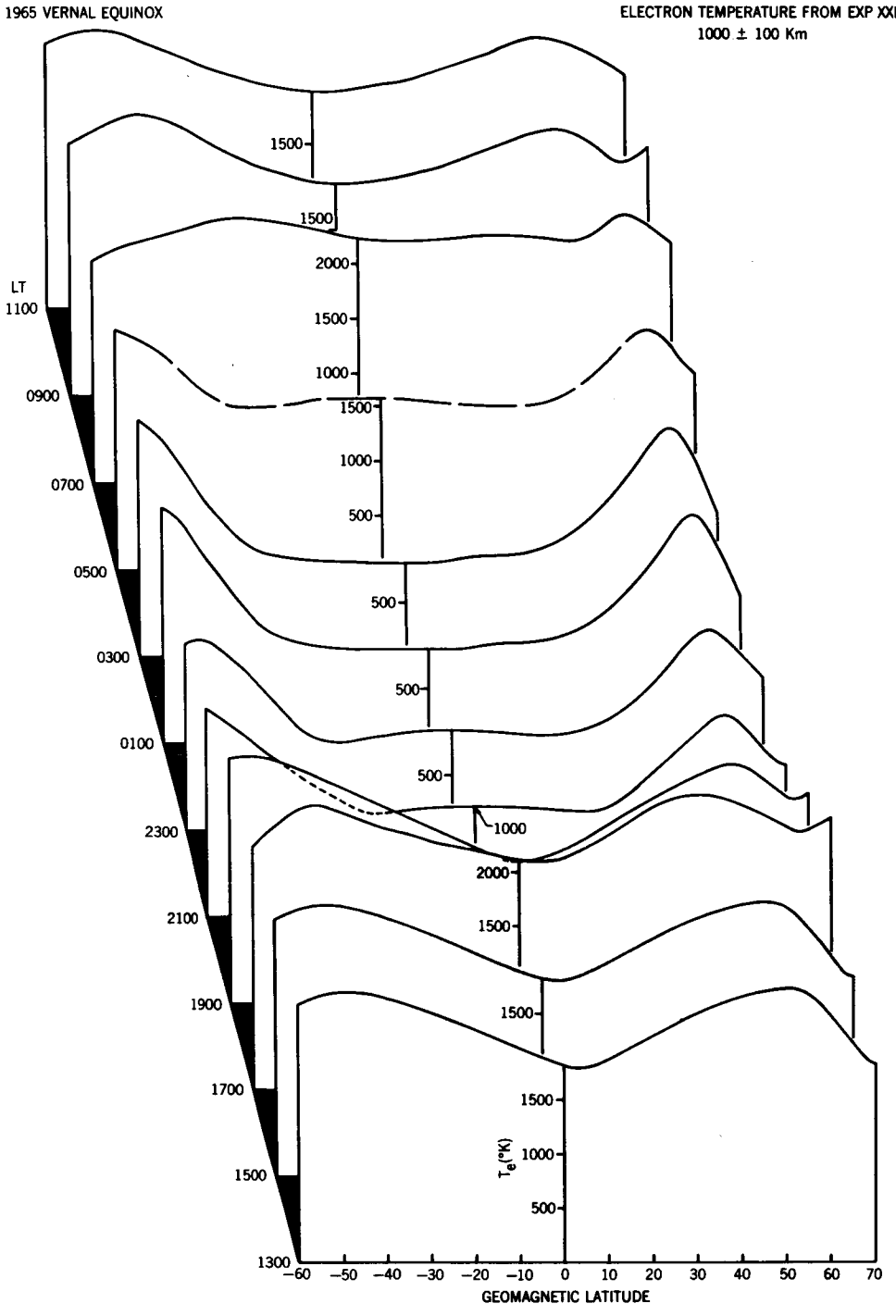

Figure 11 – Averaged latitudinal and local time behavior of T_e at 1,000 kilometers near vernal equinox. The long dashes (0500 hours) indicate that this curve was in part interpolated from curves as sufficient data to fully define it were not available in that period.

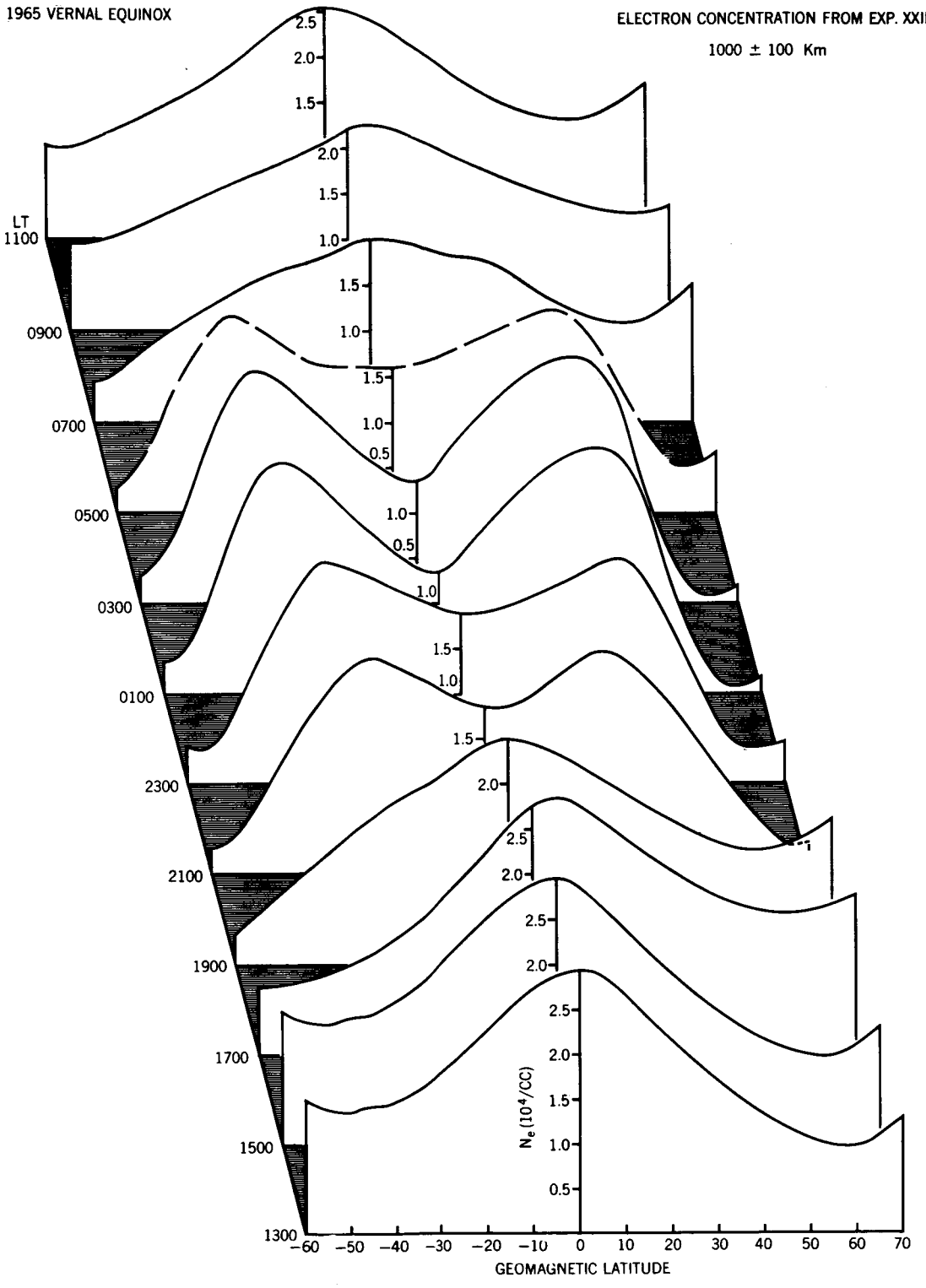

Figure 12 – Averaged latitudinal and local time behavior of T_e corresponding to N_e data of figure 11.

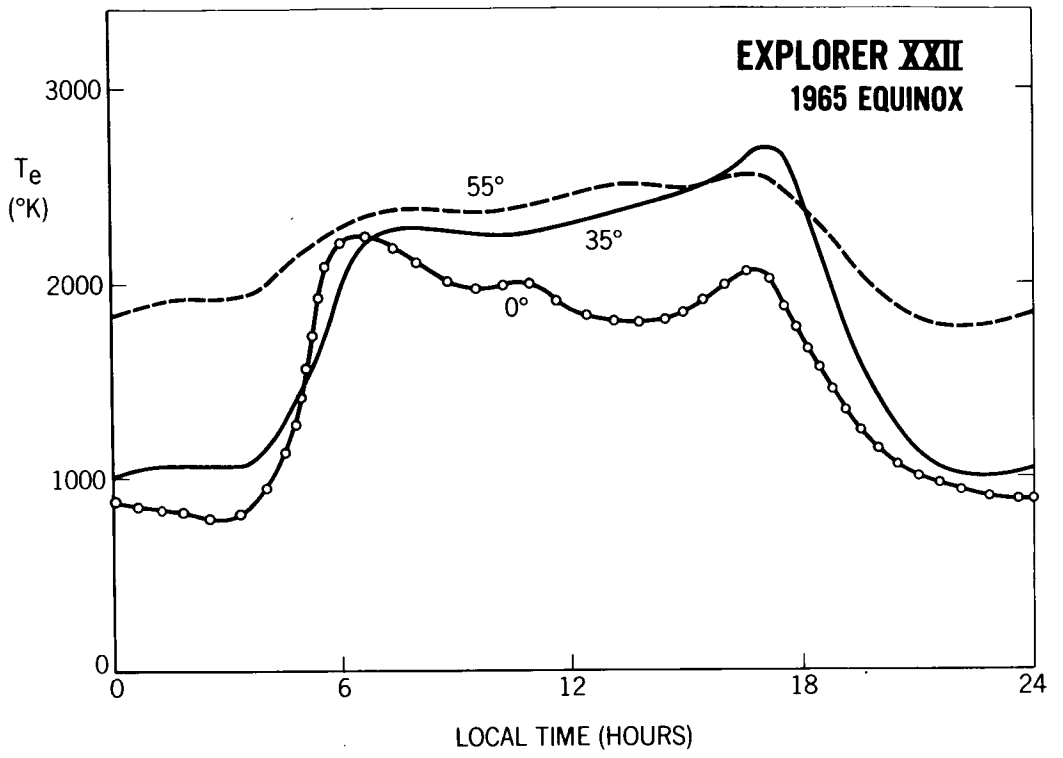

Figure 13 – Averaged diurnal variation of T_e at magnetic latitudes of 0°, 35°, and 55°, at the 1,000 kilometer level, near equinox.

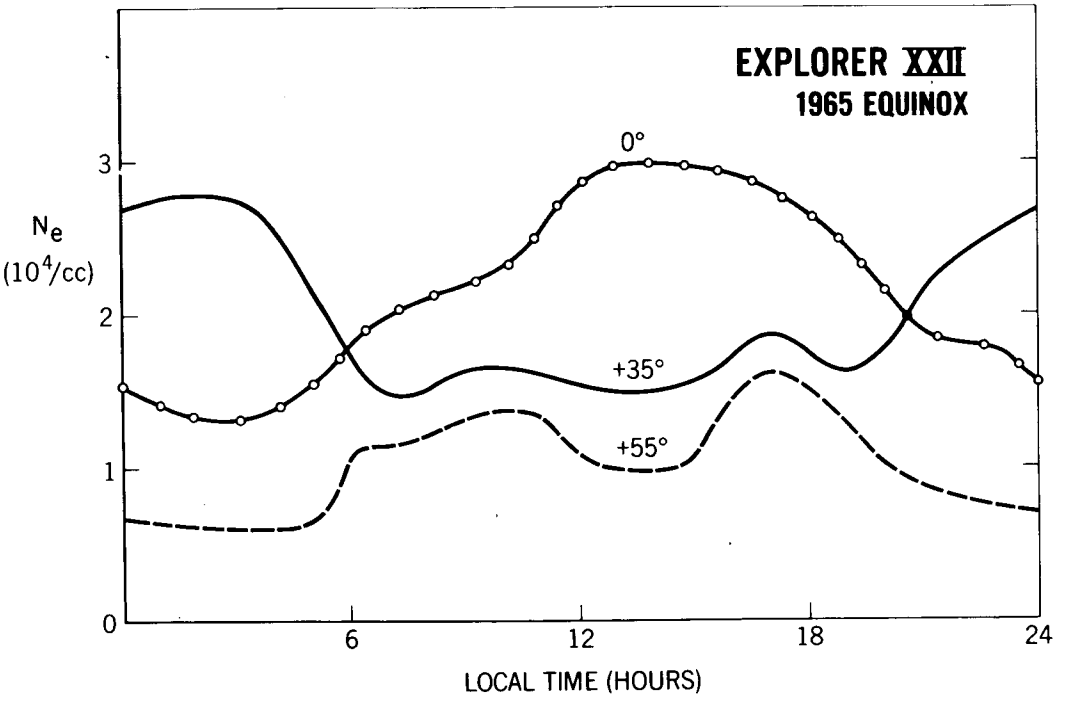

Figure 14 – Averaged N_e behavior corresponding to T_e data of figure 13.

It is, of course, realized that diurnal and seasonal effects are not entirely uncoupled in this kind of display, especially for the higher latitudes where seasonal variations are very important. However, the two effects can be largely unscrambled by comparing the data from similar local times at different seasons.

Since details of the diurnal behavior cannot be accurately resolved from the three-dimensional drawings such as figures 9 - 12, we have replotted the equinox data on a local time scale for three representative magnetic latitudes. These are shown in figures 13 and 14.

DISCUSSION OF THE RESULTS

In this section we will point out what appear to be the most significant features of the 1,000 kilometer ionosphere and discuss their implications qualitatively. In a subsequent section, more quantitative interpretation of selected parts of the data will be presented.

Several prominent features of the topside ionosphere are evident in figures 9 through 12 and should be noted specifically. These include the latitudinal, diurnal and seasonal behavior, all of which clearly exert a major influence upon the structure of the ionosphere at this altitude.

Latitudinal Variations:

As evident in earlier Explorer XXII results (Brace and Reddy, 1965) the latitudinal distributions of N_e are characterized by a strong equatorial maximum in the daytime and a pair of middle latitude maximums at night. The corresponding latitude profiles of T_e exhibit more or less uniformly high temperatures in the daytime, but a deep low latitude trough develops at night. A smaller, but

still well defined, equatorial minimum of T_e observed throughout the day is an important feature whose significance will be discussed in a later section.

Diurnal Variations:

The transitions between the daytime and nighttime structure occur in an extremely regular fashion which can best be visualized in the equinox data which is relatively free of seasonal asymmetries between the opposite hemispheres (figures 11 and 12).

As mentioned above, the midday T_e profile (1300 hours) exhibits more or less uniformly high temperatures, except for a shallow minimum at the equator. At sunset the equatorial T_e falls very rapidly to form a deeper minimum which spreads poleward throughout the night. By 2300 hours T_e is uniformly low between 40° north and south latitudes, having a value only slightly above the expected neutral particle temperature of about 700°K.

Simultaneous with the sunset decline in T_e the equatorial maximum of N_e gives way to an equatorial trough which also deepens and widens through the night. Concurrent with the sunset development of the equatorial trough an enhancement of N_e occurs at middle latitudes so that the nighttime concentration exceeds the daytime value there. This sunset transition for the vernal equinox is best illustrated in figure 15 which shows the deepening of the T_e minimum and the development of the N_e trough.

Figure 16 shows a similar sequence describing the dawn transition. At ground sunrise (0500 - 0600), the electron temperature increases rapidly, but in a complex pattern, throughout the trough region, T_e becoming more or less

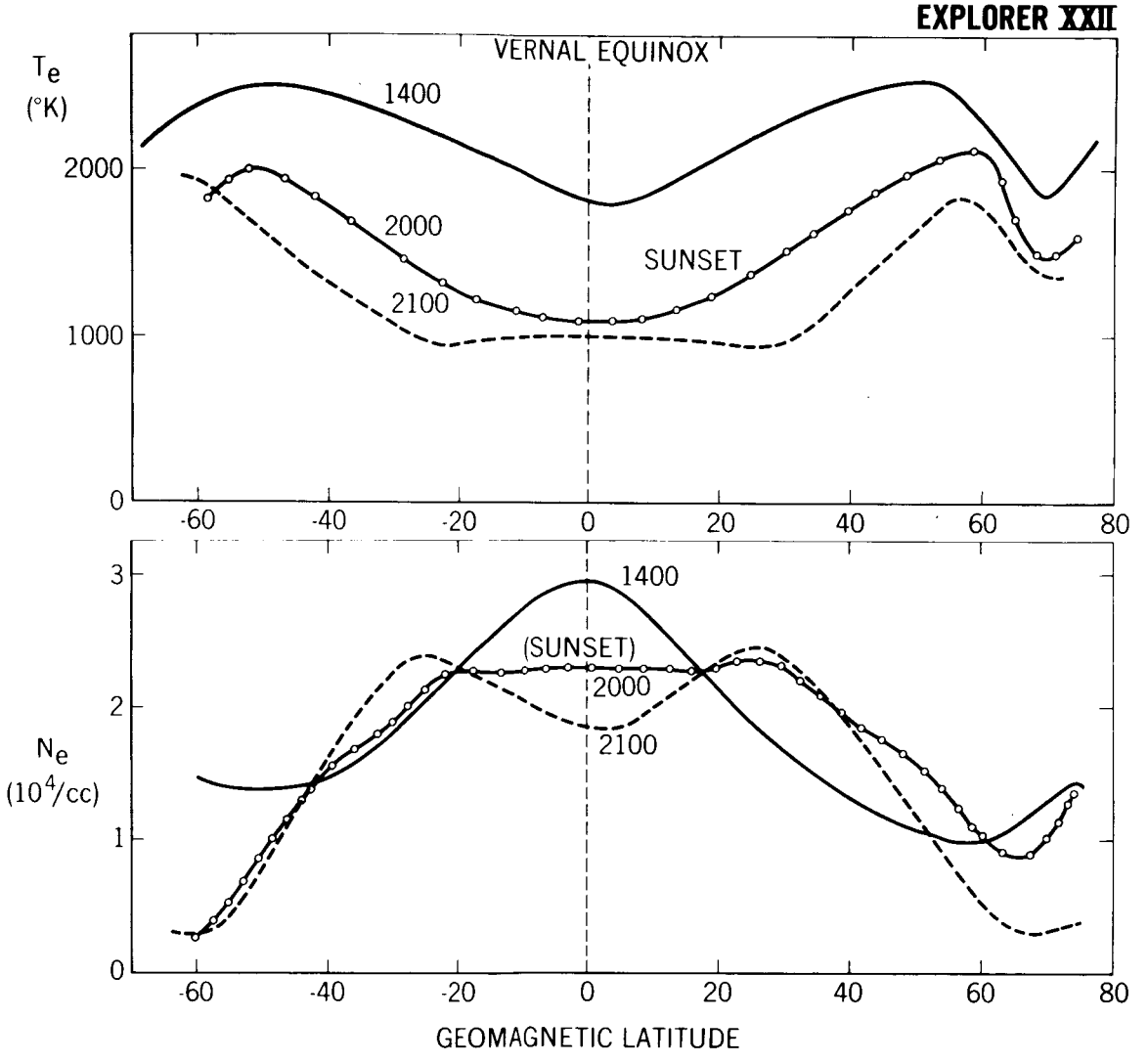

Figure 15 – T_e and N_e during sunset transition at vernal equinox at 1,000 kilometers.

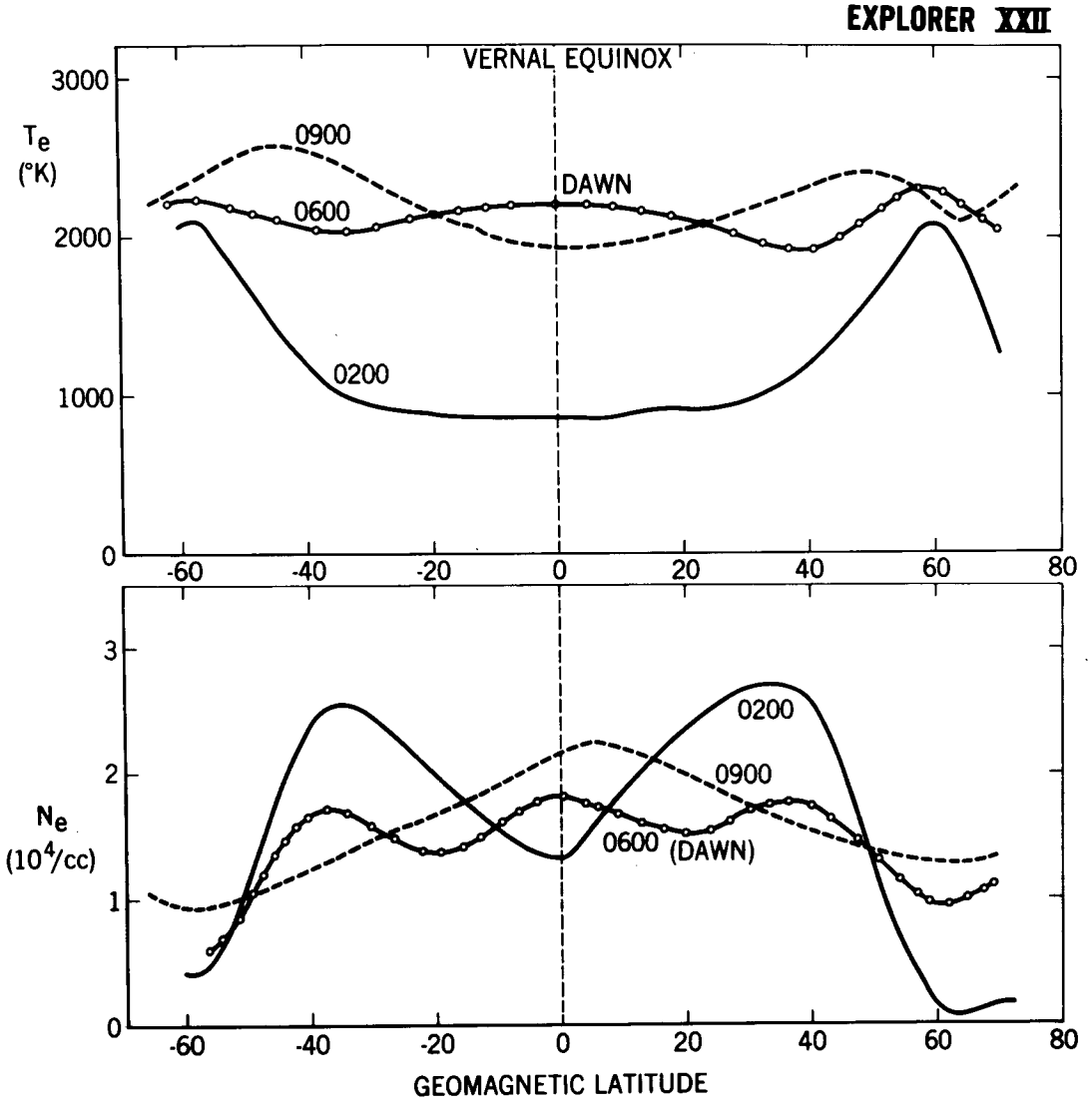

Figure 16 – T_e and N_e during sunrise transition.

uniformly high (2,000 - 2,500°K) at all latitudes soon after dawn. The corresponding behavior of N_e in this dawn transition is particularly interesting. In response to the dawn increase of T_e (0600 hours) the midlatitude N_e maximums decrease drastically and an equatorial maximum appears between them. Only at this time are all three N_e features evident. By 0900 hours, the daytime maximum is well developed and the nighttime maximums have disappeared.

Seasonal Effects:

Several seasonal effects are evident, both within the "equinox period," and when solstice and equinox data are compared. As one expects there is a marked symmetry of N_e and T_e about the magnetic equator in the equinox period. This symmetry is especially evident in the 0900 and 2100 hour data which corresponded to the actual time of equinox as evident in figure 8. Other local times may have occurred as much as six weeks before or after equinox. In contrast to this symmetry at equinox, the 1700 and 1900 hour data measured in mid-April show an appreciable enhancement of N_e in the summer hemisphere. The solstice data in figures 9 and 10 show this seasonal asymmetry even more strongly.

It is probably significant that the position of the N_e maximum itself remains within 5° of the magnetic equator in spite of the fact that the declination of the sun relative to that equator may be as great as 35°. This magnetic symmetry suggests that the magnetic control of the charge transport processes is more important than the zenith angle control of the production processes below.

Another seasonal effect is evident in the different manner in which the dawn and sunset transitions occur at solstice and equinox. At equinox (figure 12), the dawn and sunset transitions proceed with magnetic symmetry, while at solstice

(figure 10) the nighttime trough develops quite differently. The daytime equatorial maximum, which is already seasonally distorted, seems to drift toward the summer hemisphere at sunset to become the nighttime maximum. Simultaneously the nocturnal maximum in the winter hemisphere simply appears as an enhancement of the already low daytime N_e profile. This asymmetry is undoubtedly related to the different times of sunset in the winter and summer hemispheres.

The Dynamic Region:

An important feature of the 1,000 kilometer level is that the low latitude region (±40°) exhibits much more diurnal variation than the middle and high latitude regions. For example, the total diurnal variation of T_e and N_e at 50° is less than 50% while these parameters vary by a factor of 3 at the equator from day to night. This "diurnal breathing" of the low latitude region is particularly evident in the equinox data of figure 12 in which the evening formation and dawn disappearance of the equatorial trough is graphically displayed.

INTERPRETATION OF RESULTS

In the earlier Explorer XXII paper, Brace and Reddy (1965) attempted to explain this diurnal breathing of the protonosphere by assuming that the protonosphere could be considered a charge-conserved system in which the movement of charge was constrained by the geomagnetic field and the proton diffusion barrier (Hanson and Ortenburger, 1961) which effectively isolates the protonosphere from the ionosphere. In such a system, the diurnal heating and cooling of the electrons and ions would induce corresponding diurnal redistribution of the charge along the field. This appeared to explain, qualitatively, the noon and midnight observations then available from Explorer XXII. The equatorial

maximum of N_e was explained as an enhancement due to a field aligned upward diffusion of electrons and ions in response to the daytime heating of the ambient electrons by escaping photoelectrons (Hanson, 1963). Conversely, the equatorial minimum of N_e was conceived as caused by downward diffusion of electrons and protons in response to the observed nighttime cooling by thermal conduction to the lower F-region. Similarly, the nighttime enhancement of N_e at middle latitudes (30° - 40°) was attributed to a downward motion of protons along the corresponding field lines with a resultant buildup of protons in the region immediately above the proton diffusion barrier which would not permit their passage to the lower F-region.

The reduced diurnal variation of N_e at slightly higher latitudes (50°) is consistent with the smaller variation of T_e observed there. It was suggested that the heat content of the field tubes above $L = 2$ (latitude of 45°) was too great to be conducted away in a single night and that this was the probable cause of the high temperature and small diurnal variation observed at higher latitudes. The shorter field tubes at lower latitudes have correspondingly less heat content, owing to their lower total electron content. Therefore one should expect an increasingly greater diurnal variation at lower latitudes as more of the heat content is drained away at night. This also implies that the short field lines, which pass through the 1,000 kilometer level above the equator, will cool most rapidly after sunset; and the region of low electron temperature will expand in a wave-like manner toward higher latitudes where the field lines are longer and take longer to cool.

Precisely this T_e behavior is observed, as especially evident in the equinox data of figure 11. Although quantitative analysis of the decay times has not yet been carried out, the qualitative agreement demonstrated here supports heat conduction from the protonosphere as a mechanism for heating the nighttime F-region. This process was first proposed as a nocturnal heat source for the F-region by Geisler and Bowhill (1965).

An apparent inconsistency in the earlier interpretation was the increased diurnal variation of N_e above 50° in spite of the small variation of T_e. It was concluded that this could not be caused by a redistribution of charge in the protonosphere, whose temperature was not changing. Furthermore, satellite measurements of ion mass (Bowen, et al., 1964a) showed that we were no longer in the protonosphere at high latitudes. Therefore it was concluded that the variations of N_e were controlled by the production, loss and heating processes of the F-region below and should not necessarily correlate with the T_e variations near the ionosphere-protonosphere boundary.

In summary, it appears that there is nothing in the more extensive results presented here which is obviously inconsistent with the explanation given earlier by Brace and Reddy (1965) of the limited amount of data then available. On the other hand, the availability of the full diurnal and seasonal behavior permits a much more comprehensive study than was then possible to test the consistency of these results with the explanation given. For example, important questions which these data may help resolve are, (1) how good is the assumption of a perfect diffusion barrier, and (2) are the temperature decay times, observed as a function of latitude, consistent with the expected electron content along the corresponding field tubes? These questions are being studied.

Background and Assumptions:

There are a number of facts about the protonosphere which appear to be well established and will be assumed true for further interpretation of the data.

Thermal Equilibrium — In view of the good thermal contact between ions and electrons and the relatively tenuous neutral atmosphere at 1,000 kilometers, one can expect the ion and electron temperatures to be equal (Evans, 1964) (Bowles, et al., 1962). In general they will exceed the gas temperature due to the selective heating of the electrons (Hanson and Johnson, 1961; Dalgarno et al., 1963; Hanson, 1963). This has been confirmed by many forms of measurements (Boggess, Brace and Spencer, 1959; Bowen, et al., 1964b; Willmore, 1965; Spencer, et al., 1965; Brace, et al., 1965).

Heat Sources for the Protonosphere — The neutral atmosphere is so tenuous at 1,000 kilometers that little solar ultraviolet energy is absorbed locally by photoionization of neutrals. At higher latitudes particle fluxes, either trapped or precipitated, are likely to be an important source of electron heating through coulomb collisions. At middle and low latitudes, with which we are concerned here, it is probable that photoelectrons are the dominant heat source for the topside ionosphere (Hanson, 1963) (Brace, et al., 1965).

When the neutral atmosphere is illuminated by solar ultraviolet, an upward flux of fast electrons (10 eV range) escapes the lower atmosphere and travels along field lines toward conjugate points in the opposite hemisphere. The escape level is near 300 kilometers, and the fluxes lie in the range of 10^8 to $10^9/cm^2/sec$ (Hinteregger, et al., 1964). These fast electrons are not trapped but make a

single transit toward the conjugate F-region, losing small increments of their escape energy in collisions with the ambient electrons encountered along the way.

It is instructive to consider the chances of a 10 eV electron reaching the 1,000 kilometer level at the conjugate point. The mean free path of a 10 eV electron moving in the protonosphere is of the order of 10^4 kilometers, which corresponds approximately to the length of a field line at 40°. Thus it can be said that photoelectrons escaping at latitudes lower than 40° can be expected to arrive at their 1,000 kilometer conjugate points with most of their original energy, which is then dissipated in the lower ionosphere. Thus, at low latitudes, one expects both an upward and downward flux to be available for impact heating of the protonosphere in the daytime.

At latitudes higher than 40° an increasing number of photoelectrons will not reach the conjugate region, and nearly all of their energy will go into heating of the protonosphere. However, only the upward flux of photoelectrons will pass the 1,000 kilometer level and be effective in heating the ionosphere there.

In this paper, the photoelectron heating will be designated as energy gain (G), and following Dalgarno et al. (1963) is given by

$$G = k_1 \, j_{ph} \, N_e/W \tag{1}$$

where

$k_1 = 1.95 \times 10^{-12}$ eV^2 cm^2
j_{ph} = flux of photoelectrons
W = energy of the photoelectrons

Cooling Mechanisms — Electron thermal conduction is the most effective cooling mechanism for the 1,000 kilometer ionosphere (Geisler and Bowhill, 1965). It appears, however, that in the daytime equatorial protonosphere, local cooling to neutral hydrogen via protons may be of greater importance.

The transfer of energy through thermal conduction parallel to the magnetic field, which may constitute either a heating or cooling, is given by

$$\text{div } j_e = \text{div } (-k_2 T_e^{5/2} \partial T_e / \partial s) \tag{2}$$

where

j_e = electron heat flux
$k_2 = 7.7 \times 10^5$ eV cm^{-1} sec^{-1} deg$^{-7/2}$
s = distance along the field line

The local cooling, L, is given by (3) when $T_e = T_i$,

$$L \propto N_e N_n (T_e - T_n) \tag{3}$$

where

N_n = concentration of neutral particle coolant
T_n = neutral temperature.

In summary, we will assume that the important processes controlling the 1,000 kilometer ionosphere will be the photoelectron heat source, the local cooling, and electron thermal conduction. Furthermore, we assume $T_e = T_i$.

Organization of the discussion:

In the remainder of the paper we will employ the energy and charge continuity equations, and the equation of motion, to test selected portions of the

Explorer 22 measurements to determine whether the processes considered here are capable of causing the observed diurnal and latitudinal behavior. Some of the features we will consider are:

1. The daytime temperature minimum at the magnetic equator, and how it is related to the maximum of N_e observed there.
2. The nighttime N_e minimum at the equator and its relation to the broad region of low T_e found there.
3. In the sunset and sunrise periods, the time derivatives of N_e and T_e and their consistency with the available heat source and cooling processes.

Equation of Motion:

If we assume that ions and electrons have much greater mobility along the magnetic field than across it, the equation describing the motion of ion - electron pairs has the form,

$$m_i N_e \partial v/\partial t + m_i N_e v \partial v/\partial s = -2k T_e \partial N_e/\partial s - 2k N_e \partial T_e/\partial s - m_i N_e g \sin I - K N_e v \quad (4)$$

where

m_i = ion mass
v = macroscopic velocity of ion - electron pairs along magnetic field
g = gravitational acceleration
I = dip angle
s = distance along the field

The term $KN_e v$ represents the ion-neutral drag, assuming the gas to be in diffusive equilibrium. This is unlikely to be important at 1,000 kilometers.

The Charge Continuity Equation:

The charge continuity equation is

$$\partial N_e/\partial t = -\partial/\partial s\ (N_e\ v) \tag{5}$$

which becomes

$$\partial N_e/\partial t = v\ \partial N_e/\partial s - N_e\ \partial v/\partial s \tag{6}$$

Energy Continuity Equation:

The energy continuity equation relating the local plasma parameters is

$$3k\ \partial/\partial t\ (N_e T_e) = \partial/\partial s\ (k_2\ T_e^{5/2}\ \partial T_e/\partial s) - (L - G)$$

which becomes

$$= k_2\ T_e^{5/2}\ \partial^2 T_e/\partial s^2 + 5/2\ k_2\ T_e^{3/2}\ (\partial T_e/\partial s)^2 - (L - G) \tag{7}$$

This expresses the time variation of the energy content of both the electrons and ions in terms of the local cooling, L, and heating, G.

It is possible to apply equations (4), (5), and (6) to the Explorer XXII data to evaluate the relative importance of the heat conduction, gain and loss processes, however it is important to note that the derivatives in these equations are taken with respect to s. Therefore only values of T_e and N_e measured along a field line are applicable. In the polar near circular orbit of Explorer XXII, this focuses our attention on the measurements taken near the magnetic or dip equator where the path of the satellite is very nearly parallel to the field.

Specialization of Equations to Equator Case:

In this section the equations of motion and continuity will be simplified to the equilibrium conditions under which they will be used; namely, at the equator at equinox when

$$\partial T_e/\partial s = \partial N_e/\partial s = v = I = 0 \tag{8}$$

At equinox, (8) holds approximately throughout the diurnal cycle but is a very good approximation at noon and midnight. Assuming (8), employing the relation

$$\partial/\partial s\,(g \sin I)_{\text{Equator}} = -2g/r, \tag{9}$$

where r is the geocentric distance, and differentiating the motion equation (4) yields

$$\begin{aligned} m_i N_e\,(\partial^2 v/\partial s \partial t) + m_i N_e\,(\partial v/\partial s)^2 + K N_e\,\partial v/\partial s = \\ -2k T_e(\partial^2 N_e/\partial s^2) - 2k N_e\,(\partial^2 T_e/\partial s^2) + \frac{2m_i g N_e}{r} \end{aligned} \tag{10}$$

Similarly, the continuity equation (7) becomes

$$\partial N_e/\partial t = -N_e\,\partial v/\partial s \tag{11}$$

which differentiated with respect to time yields

$$\partial^2 N_e/\partial t^2 = -N_e\,\partial^2 v/\partial s \partial t \tag{12}$$

Finally, employing (11) and (12), the motion equation (10) becomes

$$-m_i\,\partial^2 N_e/\partial t^2 + m_i\,N_e\,(\partial N_e/\partial t)^2 + K(\partial N_e/\partial t) = -2k\,T_e(\partial^2 N_e/\partial s^2) - 2k\,N_e(\partial^2 T_e/\partial s^2) + \frac{2m_i\,g\,N_e}{r}. \tag{13}$$

Similarly, the energy equation (7) becomes

$$2k(T_e\,\partial N_e/\partial t + N_e\,\partial T_e/\partial t) = k_2\,T_e^{5/2}\,\partial^2 T_e/\partial s^2 - (L - G) \tag{14}$$

Equations (13) and (14) are particularly well suited for application to Explorer XXII equatorial results because they contain only terms which can be derived directly from the measurements of T_e and N_e and their temporal and spacial derivatives. In the following sections, we shall employ these equations to investigate two different situations at the equator; (1) the sunset period in which strong time variations occur and (2) the steady state periods near noon and midnight in which the time derivatives vanish.

APPLICATIONS TO EXPLORER XXII RESULTS:

The Sunset Period

The post-sunset situation is in one respect very simple since the energy gain, G, from fast photo electrons is negligible. It is clear from the latitudinal profiles at sunset (figure 12) that $\partial^2 T_e/\partial s^2$ is positive at the equator; i.e., there is always a T_e minimum at sunset. Furthermore, $\partial T_e/\partial t$ and $\partial N_e/\partial t$ are always negative near sunset at the equator, as shown in figure 17. Therefore the left side of (14) is negative, which implies that the local energy loss, L, via ions to neutrals must exceed the energy conducted into the equatorial region. Thus an

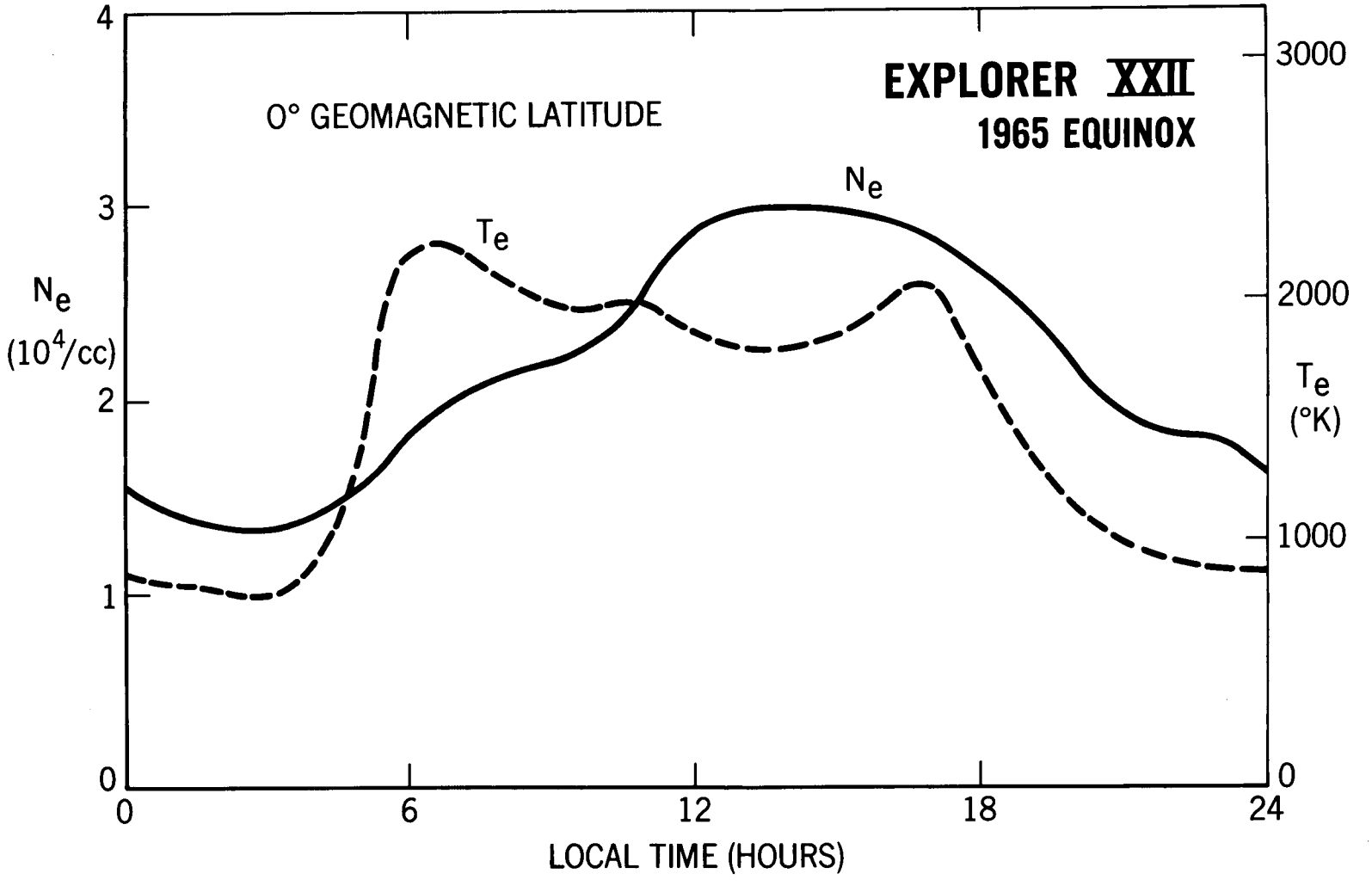

Figure 17 – Diurnal variation of T_e and N_e at the magnetic equator at 1,000 kilometers.

important result is that local cooling governs the energy variation in the sunset period. It is interesting that electron heat conduction at 1,000 kilometers at low latitudes is actually upward along the field lines into the equatorial region rather than downward into the lower F-region. There may, however, be a temperature maximum at a lower altitude along the field line from which heat would be conducted downward. This is true not only at sunset but throughout the day as well.

The next question is what ions and neutrals are responsible for the local cooling. The direct measurements of ion composition on the OGO-A and OGO-C satellites show that H^+ is clearly the dominant ion at 1,000 kilometers at the equator (Taylor, et al., 1965) (Taylor, et al., 1966). Local cooling of electrons depends very sensitively upon the ion and neutral composition, the lighter ions and neutrals being particularly effective in cooling the electrons. For example H is about 10 times as effective as H_e in cooling a H^+ and electron plasma. At the present low levels of solar activity, the neutral atmospheric models (see for example Harris and Priester, 1964) expect H and H_e to be the major neutrals at 1,000 kilometers, with a H_e concentration of about 5×10^5/cc and an H concentration of about 3×10^4/cc. Thus considering their relative effectiveness for cooling, either could be the major cooling agent. The accuracy of this H_e concentration has been confirmed by the direct measurements from Explorer XVII (Reber and Nicolet, 1965), however, the amount of neutral hydrogen is actually quite uncertain.

If we assume that hydrogen is the most important coolant the local loss term (3) becomes

$$L = k_3 N_H N_e (T_e - T_N) \tag{15}$$

where

$$k_3 = 4 \times 10^{-13} \text{ eV cm}^3 \text{ sec}^{-1} \text{ deg}^{-1}$$

and we can estimate the amount of H required to produce the sunset decline of the energy content. Assuming again $G = 0$, and using the Explorer XXII values for T_e, N_e, and their time derivatives in (14), we find that about 5×10^5/cc atoms of hydrogen are required to produce the observed cooling. This is about a factor of ten higher than given by the models and suggests that H_e and H are present in about equal abundances at 1,000 kilometers at low levels of solar activity. Ten times this amount of H_e would be required to produce the same cooling rate, and this is not in accord with direct measurements (Reber and Nicolet, 1965) at a comparable level of solar activity. We will see in a later section that a similar amount of H is required to produce the daytime T_e minimum observed at the equator.

Diffusive Equilibrium

A second approach to the analysis of the dynamic period near sunset is through application of the diffusion equation (13). When the individual terms in (13) are evaluated, by the use of Explorer XXII data and other measurements of m_i, it is found that the magnitude of each of the terms on the left is at least a factor of a hundred smaller than each term on the right. This means that the terms on the right are in balance and we have the statement of diffusive equilibrium

$$0 = -2k T_e \partial^2 N_e / \partial s^2 - 2k N_e \partial^2 T_e / \partial s^2 + \frac{2 m_i g N_e}{r} \tag{16}$$

Thus, even during periods of strong dynamic variation, diffusive equilibrium is found to hold at 1,000 kilometers at the equator. We will employ this fact in the next section.

Diffusive Equilibrium in The Steady State Case

The second situation which lends itself to straight-forward analysis is the equilibrium period corresponding to midday or midnight. Figures 18 and 19 represent the N_e and T_e distributions at these times and show the total diurnal excursion of these parameters at moderate latitudes. In this section, we will examine the temporal variation of N_e at the equator and the latitudinal variation itself.

Since we have shown diffusive equilibrium to exist, we employ equation (16) in the following form to see if the latitudinal profiles of N_e and T_e are consistent with diffusive equilibrium,

$$1/N_e \, (\partial^2 N_e/\partial s^2) = 1/T_e \left(\frac{m_i \, g}{k \, r} - \partial^2 T_e/\partial s^2\right) \qquad (17)$$

Daytime Data — Employing the midday equinox data shown in figures 18 and 19, and assuming H^+ ions, we find that the term $m_i g/k r$ is about equal to the term $\partial^2 T_e/\partial s^2$, at the equator, thus permitting $\partial^2 N_e/\partial s^2$ to be either positive or negative. Therefore, we can say that the observed latitudinal variation of T_e would permit either a small maximum or small minimum of N_e at the equator. However, a similar calculation employing the corresponding T_e data at the time of solstice shows that (17) is clearly negative at this time, and a strong N_e maximum can be expected at the equator. These results are consistent with the

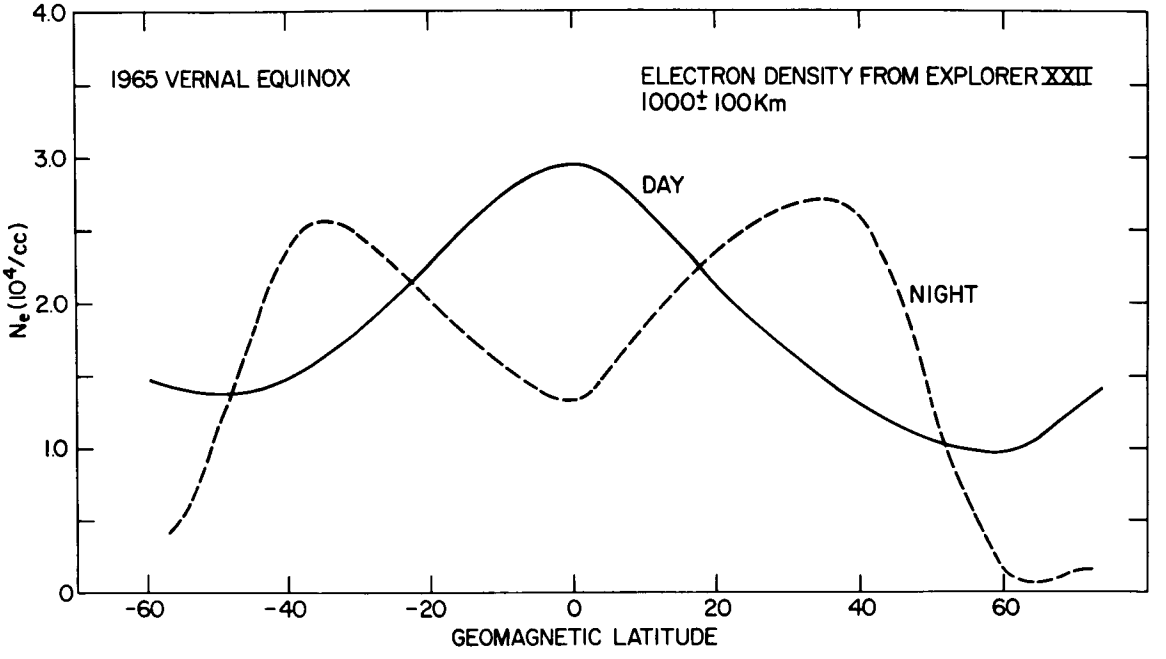

Figure 18 – Total diurnal variation of N_e as a function of latitude at vernal equinox.

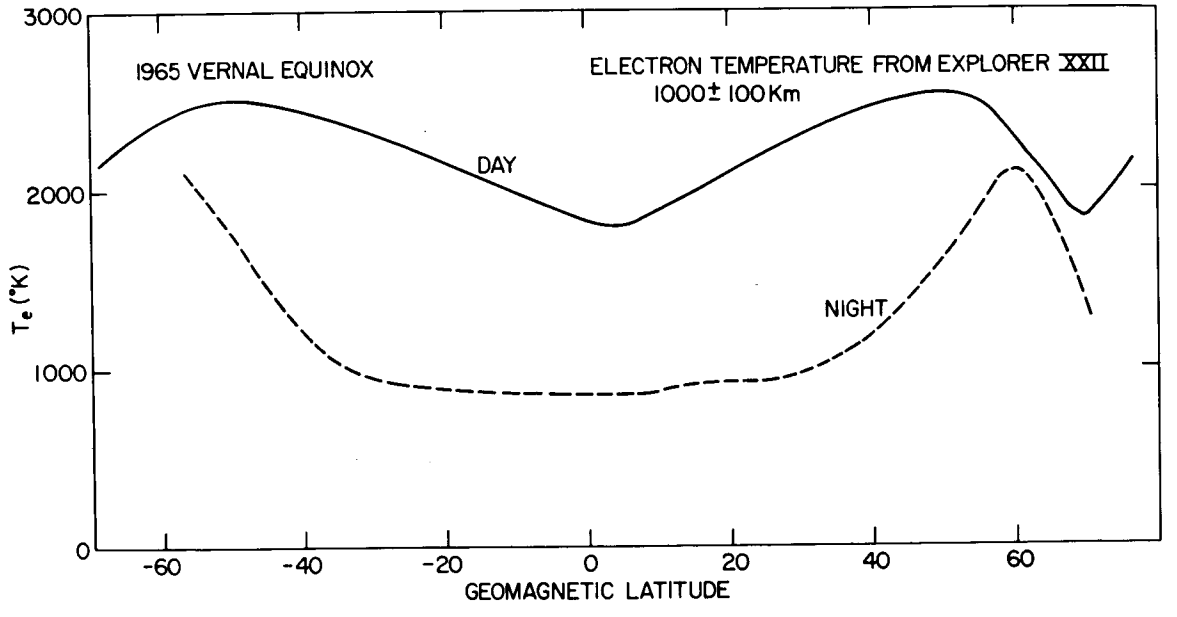

Figure 19 – Total diurnal variation of T_e corresponding to N_e data of figure 18.

observations of N_e which show a stronger maximum at the equator at the solstice than at the equinox.

At this point, it is important to realize that we have not explained the equatorial maximum of N_e, but have merely shown that the latitudinal distributions of T_e and N_e near the equator are self consistent through the equation of diffusive equilibrium. The causes for the existence of the N_e maximum clearly must lie in the causes of the T_e distribution, itself. As suggested earlier the low equatorial values of T_e are produced by the enhanced local cooling which in turn results from the abundance of H+ ions in the equatorial region. The predominance of the light ions further enhances the equatorial maximum through the mass dependence in the diffusion equation (17). Thus, it appears that the explanation of the behavior of the 1,000 kilometer level lies in the composition-determining processes occurring in the regions below, probably the most important of which is the oxygen hydrogen charge exchange process.

Nighttime data — Repeating the diffusive equilibrium test for the nighttime equatorial results shown in figures 18 and 19, we find that $\partial^2 T_e / \partial s^2$ vanishes in the flat nighttime trough. Therefore, one can expect to find an N_e trough, which of course is observed. The calculated value of $\partial^2 N_e / \partial s^2$ also agrees quantitatively with the shape of the observed N_e trough.

Energy Continuity in the Daytime Steady State

We now apply the energy continuity equation (14) to the daytime equatorial data as a check upon the hydrogen result of similar calculations using the post-sunset data in which G was assumed zero.

The precise calculation of photoelectron heating becomes quite complex since it involves a detailed knowledge of the energy distribution of the photoelectrons and the ambient electron concentration distribution along the field line. For our purposes, however, it will be adequate to employ the simpler description of the process given by Dalgarno et al. (1963), who shows that for electron energies greater than 3eV, the energy dissipation to the ambient electrons is described by

$$\partial W/\partial s = -k_1 N_e/W \tag{18}$$

Assuming a flux of fast electrons, j_{ph}, traveling along the field experiencing negligible loss of energy, $(\partial j_{pn}/\partial s = 0)$, we find

$$G = -2\,\partial(j_{ph} W)/\partial s = 2k_1\, j_{ph}\, N_e/W \tag{19}$$

The factor of two includes the photoelectrons traveling upward from both sunlit hemispheres which are available for heating electrons at the 1,000 kilometer level. Substituting this gain term (19) and the loss term (15) into the energy continuity equation (14), and assuming a steady state condition $(\partial/\partial t = 0)$ we arrive at

$$k_2\, T_e^{5/2}\, (\partial^2 T_e/\partial s^2) + 2k_1\, j_{ph}\, N_e/W - k_3\, N_H\, N_e\, (T_e - T_N) = 0 \tag{20}$$

If we assume a mean photoelectron energy of 10eV and employ the measured daytime equatorial values of T_e and N_e, it is possible to relate the photoelectron flux, j_{ph}, to the amount of hydrogen required to reproduce the observations. From the measurements of the Hinterregger, et al. (1964) and Mularchik and

Vaisberg (1964), it appears that a fast electron flux of about 5×10^8 cm^{-2} sec^{-1} is available for heating. This flux requires the amount of cooling which would be provided by a neutral hydrogen concentration of 4×10^5/cc, a value which is in satisfactory agreement with that derived earlier using the energy decay rate of the post sunset period.

CONCLUSIONS

Summary of interpretation:

In the previous sections we have employed the equation of motion, and the equations of charge and energy continuity to test the equatorial (field aligned) results from Explorer XXII. As a result, we have been able to conclude that:

1. the equatorial protonosphere near 1,000 kilometers is always in diffusive equilibrium, even during the periods of most dynamic change at sunrise and sunset.
2. the daytime minimum of T_e observed at the equator is caused by local cooling via protons to an unexpectedly great amount of neutral hydrogen (about 4×10^5/cc).
3. the daytime equatorial maximum of N_e which is observed is consistent with the T_e minimum and is enhanced by the predominance of H+.
4. the flat nighttime trough of T_e is quantitatively in agreement with the steep trough of N_e found at the equator.
5. the sunset decay of T_e and N_e at the equator requires a local cooling which is also consistent with a high concentration of neutral hydrogen ($\approx 5 \times 10^5$/cc).

Although the above conclusions are derived from observations at 1,000 kilometers in the equatorial protonosphere, the processes which have been identified in this region are surely important in other parts of the protonosphere as well. However, to understand the entire latitudinal and local time behavior which is observed, a much more comprehensive study is required. In particular, the third dimension, that of altitude, must be introduced.

Measurements Needed

In the measurements area, electron temperature and concentration and ion composition data are needed for a wider range of altitudes and on a global scale. This is not easily accomplished. A single satellite cannot provide the needed latitude and local time resolution at all altitudes because of the complex manner in which the latitude, local time, season and altitude are mixed by the long term motions of the orbit; namely, the orbital precession and apsidal rotation. For example, even the high sampling density of the Explorer XXII data given here are no more than adequate to describe the behavior of the 1,000 kilometer level alone. If these samples were spread over a wide range of altitudes, the resolution of the local time, latitude, longitude and seasonal behavior at each altitude would be hopelessly diluted.

Ideally one would like to have such measurements on a number of satellites in circular orbits at several altitudes. This would permit the ionosphere to be observed simultaneously in three dimensions. This need is partly fulfilled by the topside sounder satellites which can remotely sample the altitudinal distribution of N_e below the satellite. Unfortunately, the sounders do not measure the most important parameters, ion composition and electron temperature, and

therefore do not provide the kind of data required to identify and evaluate the controlling processes.

A number of satellites, already in orbit, carry the necessary instruments for some degree of altitudinal resolution of these parameters, although their orbits do not permit unambiguous separation of the altitudinal effects from the other equally important variables. These satellites include the OGO-A and OGO-C which carry ion mass spectrometers (Taylor, et al., 1965) (Taylor, et al., 1966) and the Explorer XXXI and Explorer XXXII which carry electrostatic probes of the type employed here, as well as ion mass spectrometers. In addition, Explorer XXXII carries instruments for measuring the neutral composition and concentration which will be useful in evaluating the importance of charge exchange between oxygen and hydrogen near the lower boundary of the protonosphere. By comparing these results with the Explorer XXII data now being obtained simultaneously at 1,000 kilometers, a degree of altitudinal structure can be extracted from the other variables which are common.

In the analytical area, a number of avenues are open. One of these is a natural extention of the investigation outlined here. We have verified by use of the equatorial data that the processes controlling the equatorial protonosphere are electron thermal conduction, impact heating by photoelectrons, and local cooling; all operating under diffusive equilibrium. Although it appears that the major behavioral features of the protonosphere at middle and low latitudes can be described by employing these processes, it remains to be shown how successfully these alone can account for the more detailed behavior evident in Figures 9 through 12. Undoubtedly, any attempt to relate analytically the entire

body of satellite measurements now becoming available will require the inclusion of additional physical and chemical processes.

ACKNOWLEDGMENTS

We are indebted to Mr. Tuck Bin Lee of the Space Physics Research Laboratory of the University of Michigan for the development and preparation of the electronic system and to J. A. Findlay for its integration into the payload and prelaunch engineering support. We also thank Messrs. J. H. Sayler, G. S. Dunham, J. Johnston, F. Huie and L. Rudolph for their outstanding efforts in reduction and analysis of the data.

REFERENCES

1. Boggess, R. L., L. H. Brace, and N. W. Spencer, Langmuir Probe Measurements in the Ionosphere, J. Geophys. Res., 64, 1627-1630, 1959.
2. Bowen, P. J., R. L. F. Boyd, C. L. Henderson, and A. P. Willmore, Electron Temperature in the Upper F-Region, Proc. Roy Soc. A, 281, 526-538, 1964 b.
3. Bowen, P. J., R. L. F. Boyd, W. J. Raitt, and A. P. Willmore, Ion Composition of the Upper F-Region, Proc. Roy. Soc. A, 281, 504-514, 1964 a.
4. Bowles, K. L., G. R. Ochr, and J. L. Green, On the Absolute Intensity of Incoherent Scatter Echoes from the Ionosphere, J. Res. National Bureau of Stds., 66D, 395-407, 1962.
5. Brace, L. H., and B. M. Reddy, Early Electrostatic Probe Results from Explorer 22, J. Geophys. Res., 70, 5783-5792, 1965.
6. Brace, L. H., N. W. Spencer, and G. R. Carignan, Ionosphere Electron Temperature Measurements and Their Implications, J. Geophys. Res., 68, 5397-5412, 1963.
7. Brace, L. H., N. W. Spencer, and A. Dalgarno, Detailed Behavior of the Mid Latitude F-Region from Explorer 17 Satellite, Planet. Space Sci., 13, 647-666, 1965.
8. Dalgarno, A., M. B. McElroy, and R. J. Moffett, Electron Temperatures in the Ionosphere, Planet. Space Sci., 11, 463-484, 1963.
9. Evans, J. V., Ionospheric Temperatures During the Launch of NASA Rocket 8.14 on July 2, 1963, J. Geophys. Res., 69, 1436-1444, 1964.

10. Geisler, J. E., and S. A. Bowhill, Exchange of Energy Between the Ionosphere and the Protonosphere, J. Atmosph. Terr. Phys., 27, 1119-1146, 1965.

11. Hanson, W. B., Electron Temperatures in the Upper Atmosphere, Space Research III, 282-302, edited by W. Priester, North Holland Publishing Company, Amsterdam, 1963.

12. Hanson, W. B., and F. S. Johnson, Electron Temperatures in the Ionosphere, Memoires Soc. R. Liege, IV, 390-423, 1961.

13. Hanson, W. B., and I. B. Ortenburger, The Coupling Between the Protonosphere and the Normal F-Region, J. Geophys. Res., 66, 1425-1435, 1961.

14. Harris, I., and W. Priester, The Upper Atmosphere in the Range From 120 to 800 KM, Brought Out by the Institute for Space Studies, G.S.F.C.-NASA, 1964.

15. Hinteregger, H. E., L. A. Hall, and G. Schmidtke, Solar XUV Radiation and Neutral Particle Distribution in July 1963 Thermosphere, Presented at the Fifth Int. Space Science Symposium, Florence, May 1964, Space Res. V, Edited by D. G. King-Hele, North Holland Publishing Company, 1965.

16. Mularchik, T. M., and O. L. Vaisberg, Low Energy Electrons Measured by the COSMOS-3 and COSMOS-5 Satellites, Presented at the Fifth Int. Space Sci. Symposium, Florence, May 1964, Space Research V, Edited by D. G. King-Hele, North Holland Publishing Company, 1965.

17. Reber, C. A., and M. Nicolet, Investigation of the Major Constituents of the April-May 1963 Heterosphere by the Explorer XVII Satellite, Planet. Space Sci., 13, 617-646, 1965.

18. Spencer, N. W., L. H. Brace, and G. R. Carignan, Electron Temperature Evidence for Non-thermal Equilibrium in the Ionosphere, J. Geophys. Res., 67, 157-175, 1962.

19. Spencer, N. W., L. H. Brace, G. R. Carignan, D. R. Taeusch, and H. Niemann, Electron and Molecular Nitrogen Temperature and Density in the Thermosphere, J. Geophys. Res., 70, 2665-2698, 1965.

20. Taylor, Jr., H. A., H. C. Brinton, and L. R. Munez, First Results from OGO-C Ion Composition Experiment, Presented at the 47th Annual Meeting of the AGU, March 1966.

21. Taylor, Jr., H. A., H. C. Brinton, and C. R. Smith, Positive Ion Composition in the Magnetoionosphere Obtained from the OGO-A Satellite, J. Geophys. Res., 70, 5769-5781, 1965.

22. Thomas, J. O., M. J. Rycroft, L. Colin, and K. L. Chan, Electron Density Profiles in Ionosphere and Exosphere, Proceedings of the NATO Advanced Study Institute held at Finse, Norway, Edit. Jon Frihagen, North-Holland Publishing Company, Amsterdam, 1966.

23. Watt, T. M., Ion Distribution and Temperature in the Topside Ionosphere obtained from the Alouette Satellite, J. Geophys. Res., 70, 5849-5859, 1965.

24. Willmore, A. P., Geographical and Solar Activity Variations in the Electron Temperature of the Upper F-region, Proc. Roy. Soc. A., 286, 537-558 (1965).